J. Fluid Mech. (2012), *vol.* 711, *pp.* 411–436. © Cambridge University Press 2012
doi:10.1017/jfm.2012.399

Simulations of a double-diffusive interface in the diffusive convection regime

J. R. Carpenter[1]†, T. Sommer[1,2] and A. Wüest[1,2,3]

[1] EAWAG Swiss Federal Institute of Aquatic Science and Technology, Surface Waters – Research and Management, Kastanienbaum, CH-6047, Switzerland

[2] Institute of Biogeochemistry and Pollutant Dynamics, Environmental Sciences, ETH, Zürich, CH-8092, Switzerland

[3] Physics of Aquatic Systems Laboratory, ENAC, EPFL, Lausanne, CH-1015, Switzerland

(Received 31 October 2011; revised 20 June 2012; accepted 6 August 2012; first published online 14 September 2012)

Three-dimensional direct numerical simulations are performed that give us an in-depth account of the evolution and structure of the double-diffusive interface. We examine the diffusive convection regime, which, in the oceanographically relevant case, consists of relatively cold fresh water above warm salty water. A 'double-boundary-layer' structure is found in all of the simulations, in which the temperature (T) interface has a greater thickness than the salinity (S) interface. Therefore, thin gravitationally unstable boundary layers are maintained at the edges of the diffusive interface. The TS-interface thickness ratio is found to scale with the diffusivity ratio in a consistent manner once the shear across the boundary layers is accounted for. The turbulence present in the mixed layers is not able to penetrate the stable stratification of the interface core, and the TS-fluxes through the core are given by their molecular diffusion values. Interface growth in time is found to be determined by molecular diffusion of the S-interface, in agreement with a previous theory. The stability of the boundary layers is also considered, where we find boundary layer Rayleigh numbers that are an order of magnitude lower than previously assumed.

Key words: double diffusive convection, ocean processes, stratified flows

1. Introduction

It has been more than 50 years now since Stern (1960) demonstrated that certain configurations of temperature and salinity may develop double-diffusive (DD) instability. The DD instability is known to generate a local convective mixing of the water column, despite the overall density stratification being gravitationally stable. The conditions required for the DD instability to develop have since been generalized (e.g. Veronis 1965; Baines & Gill 1969), showing that only two density-contributing scalars with different molecular diffusivities are required, provided that one exhibits a gravitationally unstable stratification, thus providing the energy source for the instability. Two fundamentally different regimes exist depending on whether T, which we shall take as the faster diffusing scalar (not necessarily temperature), or S, slower

† Present address: Department of Geology and Geophysics, Yale University, 210 Whitney Ave., New Haven, CT 06511, USA. Email address for correspondence: jeffcarp@gmail.com

diffusing, is in a gravitationally unstable configuration. Here we shall focus on the diffusive convection regime where T is gravitationally unstable.

Numerous investigations have identified diffusive convection in the oceans (Neal, Neshyba & Denner 1969; Kelley *et al.* 2003; Timmermans *et al.* 2008) and lakes (Hoare 1966; Schmid *et al.* 2004; Schmid, Busbridge & Wüest 2010), as well as in geological processes (Huppert & Sparks 1984). In these observations the vertical T- and S-profiles are found to form thermohaline staircase structures composed of sharp high-gradient interfaces sandwiched between nearly homogeneous and turbulent mixed layers. In efforts to understand the transport mechanisms, and TS-fluxes, through these thermohaline staircases, a number of laboratory and theoretical studies chose to focus on the simpler configuration of a single interface separated by mixed layers above and below (e.g. Turner 1965; Shirtcliffe 1973; Crapper 1975; Marmorino & Caldwell 1976; Linden & Shirtcliffe 1978; Newell 1984; Fernando 1989; Kelley 1990). Despite the success of these studies in developing various 'laws' that parameterize the interfacial TS-fluxes, a basic knowledge regarding the transport mechanisms, and interface structure, is still lacking.

In the present paper we perform a series of three-dimensional direct numerical simulations (DNS) of a 'diffusive interface' in order to further elucidate the processes controlling the fluxes of T and S. The simulations are motivated by previous laboratory experiments that have been influential in our current understanding of the diffusive interface, as well as recent high-resolution microstructure observations taken in the thermohaline staircase of Lake Kivu (Schmid *et al.* 2010; Sommer *et al.* 2013). DNS has a number of advantages over both laboratory experiments and field observation, such as a precise description of the velocity and scalar fields, the possibility to evaluate exact TS-fluxes, and controlled boundary conditions. To our knowledge, this is one of the first series of fully three-dimensional DNS to be performed for the diffusive convection regime (Caro 2009), although two-dimensional DNS have been carried out previously (Molemaker & Dijkstra 1997; Noguchi & Niino 2010*a*,*b*; Carpenter, Sommer & Wüest 2012). The DNS of the present paper give us an in-depth look at the diffusive interface that has never before been attained, and allows us to test the assumptions of a number of previous theories.

The paper is organized as follows. After a description of the simulations and their relation to geophysical observations in § 2, we provide an overview of the time evolution of the flow (§ 3). The interface structure, and the large-scale circulations present, are described in § 4. The implications for the fluxes of T and S, as well as the ratio of these fluxes is discussed in § 5. A theory describing the boundary layer stability is then tested in § 6, with conclusions presented in the final section (§ 7).

2. Simulations and methods

2.1. *Simulations*

The DNS are carried out with a version of the spectral code originally described by Winters, MacKinnon & Mills (2004), which has been modified by Smyth, Nash & Moum (2005) to carry a second scalar (S) at a resolution that is twice that of the other fields (e.g. velocity, pressure, T). The code is therefore especially suited to performing DNS of oceanic DD convection, where the molecular diffusivities of T and S, denoted by κ_T and κ_S, can vary by two orders of magnitude (Kimura & Smyth 2007). These scalars both satisfy advection–diffusion equations and are related to the fluid density ρ, by a linear equation of state given by

$$\rho = \rho_0 + T + S, \tag{2.1}$$

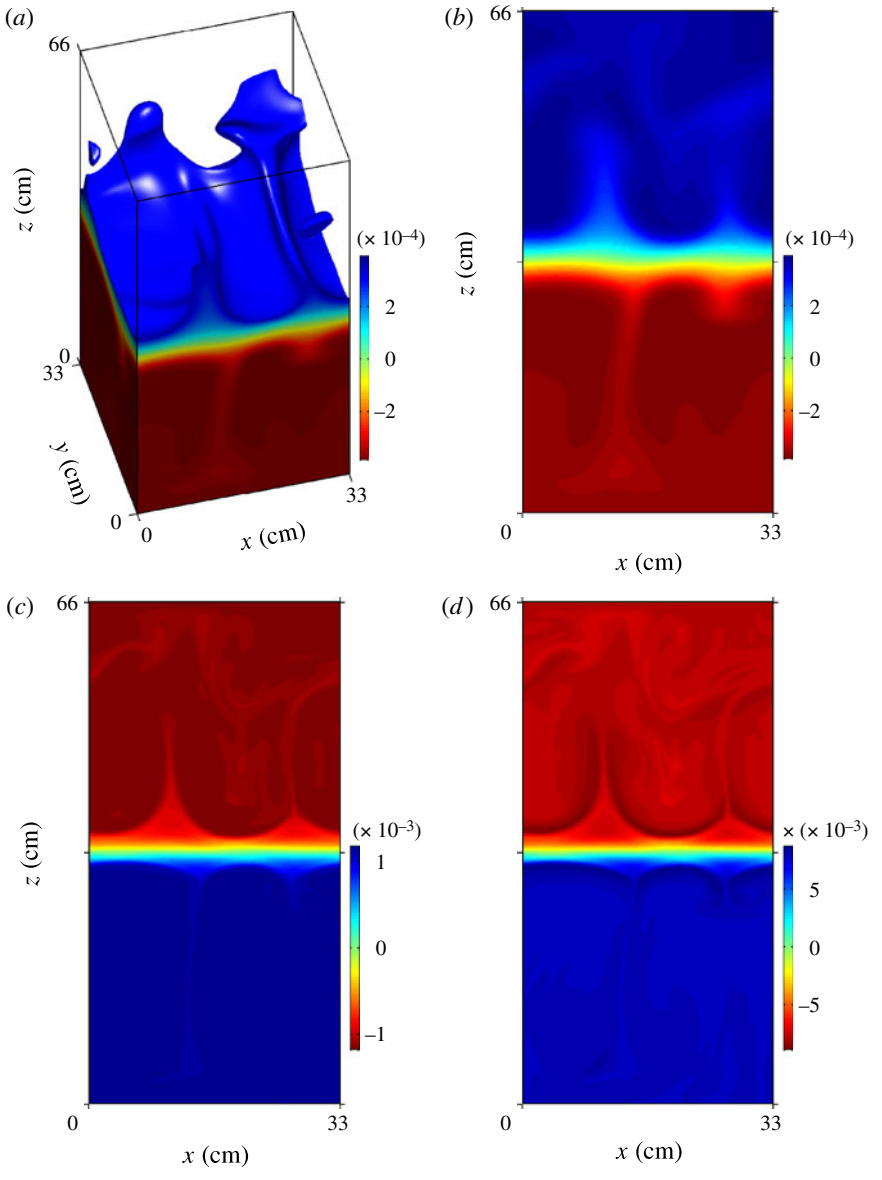

FIGURE 1. Representative plots of the T-, S-, and ρ-fields during simulation II (see table 2) at $t = 11.4$ h. (*a*) The full three-dimensional T-field with $T > 0.45\Delta T$ made transparent. The two-dimensional slices of the T-, S-, and ρ-fields shown in (*b,c,d*) respectively, are taken at $y = 0$. The units for all panels are in kg m^{-3}.

where ρ_0 is a constant reference density, and T and S are henceforth given in density units. A representative example of the T-, S-, and ρ-fields is shown in figure 1. It is possible to see that the lower κ_S leads to the development of finer-scale features and a thinner interface in S than in the much faster diffusing T (figure 1*b,c*).

The simulations solve the equations of motion for an incompressible Boussinesq fluid (Turner 1973) on a rectangular domain of size $\{L_x, L_y, L_z\}$ with an even spacing

between grid points in each of the three Cartesian coordinates; x, y in the horizontal, and z in the vertical (positive upwards). Initial conditions consist of specifying profiles of T and S given by

$$T(z) = \frac{\Delta T}{2} \tanh\left[\frac{2(z - L_z/2)}{h_0}\right] \quad \text{and} \quad S(z) = -\frac{\Delta S}{2} \tanh\left[\frac{2(z - L_z/2)}{h_0}\right], \tag{2.2}$$

where ΔT and ΔS represent the absolute change in T and S across the interface, h_0 is the initial thickness of the T- and S-interfaces, and L_z is the vertical domain height. In addition to the TS-profiles, the velocity field is perturbed with random noise at the initial time step in each of the three components (u, v, w). The noise is centred about the interface level, and serves as an initial seed for the instabilities which will eventually develop in the vicinity of the interface.

The boundary conditions chosen for the simulations are periodic in the horizontal (i.e. at $x = 0, L_x$ and $y = 0, L_y$), with a free-slip condition for the velocity field, and no-flux conditions for the scalar fields on the top and bottom boundaries (i.e. at $z = 0, L_z$). These boundary conditions mean that no heat or salt is able to escape the domain, and the T and S differences across the diffusive interface gradually decrease in time. This 'run-down' scenario is similar to a number of previous laboratory experiments that have been carried out in containers that are either insulated against the escape of heat (Newell 1984), or that have been conducted with a scalar other than heat, for example a salt–sugar system (Turner, Shirtcliffe & Brewer 1970; Shirtcliffe 1973; Stamp *et al.* 1998).

2.2. *Scales and dimensionless parameters*

Of central importance in the study of the diffusive interface are the T- and S-interface thicknesses. In accordance with numerous other studies, we shall define the interface thickness by

$$h_\varphi \equiv \Delta\varphi \Big/ \left(\frac{\partial \varphi}{\partial z}\right)_{\varphi_0}. \tag{2.3}$$

Here, and throughout the rest of the paper, φ represents both T and S, and the φ_0 subscript indicates that the derivative is taken at the location of the isoscalar (i.e. $\varphi = \text{const.}$) surface of the interface. In practice, we compute the gradient by fitting a line over the region of the interface where $-\Delta\varphi/8 < \varphi < \Delta\varphi/8$ at each (x, y) location. Assuming an error-function form of the interface, this averaging underestimates the true gradient by only 1.1 %. In addition, $\Delta\varphi$ is computed by the absolute difference between the average value of φ for the upper and lower quarters of the domain.

Given the scales defined above, it is possible to form the following independent dimensionless numbers which are characteristic of the diffusive interface:

$$Ra_I \equiv \frac{g\Delta T h_T^3}{\rho_0 \nu \kappa_T}, \quad R_\rho \equiv \frac{\Delta S}{\Delta T}, \quad Pr \equiv \frac{\nu}{\kappa_T}, \quad \tau \equiv \frac{\kappa_S}{\kappa_T} \quad \text{and} \quad r \equiv \frac{h_T}{h_S}, \tag{2.4}$$

where g is gravitational acceleration, and ν is the kinematic viscosity. These dimensionless parameters correspond to a thermal interfacial Rayleigh number, the stability ratio, Prandtl number, diffusivity ratio, and interface thickness ratio, respectively. For a given simulation, both Pr and τ remain constant since they are properties of the fluid and the scalars. However, all three of Ra_I, R_ρ, and r are changing in time due to the changing of ΔT, ΔS, h_T, and h_S. In addition to the

	Dimensional scales		Dimensionless parameters				
	ΔT (kg m$^{-3}\times10^{3}$)	h_T (cm)	Ra_I $\times10^{-3}$	R_ρ (—)	Pr (—)	τ (—)	$L_z/2h_T$ (—)
Simulations	0.2–1.2	2.0–19	12–230	2–14	6.25	0.01–0.33	1.7–25
Lake Kivu	0.5–4.8	3.5–18	3.4–890	2.2–5.1	≈6.25	≈0.01	3–22

TABLE 1. The range of parameters and scales used in the simulations, and those measured in the thermohaline staircase of Lake Kivu by Sommer *et al.* (2013). The ranges shown for Lake Kivu correspond to the 10th and 90th percentiles. For the simulations we use $\rho_0 = 997$ kg m^{-3} and $\nu = 9.0\times10^{-7}$ m^2 s^{-1}.

Simulation	Dimensions	$\{L_x, L_y, L_z\}$ (cm)	$\{N_x, N_y, N_z\}$ (—)	h_0 (cm)	R_ρ (—)	τ (—)
Dependence on τ						
I	3	33, 33, 66	320, 320, 640	5	2–9	0.01
II	3	33, 33, 66	320, 320, 640	5	2–6	0.035
III	3	33, 33, 66	320, 320, 640	5	2–5	0.07
IV	3	33, 33, 66	320, 320, 640	2	2–2.5	0.33
Dependence on domain size						
V	3	33, 33, 99	288, 288, 864	5	2–4	0.07
VI	3	66, 33, 66	576, 288, 576	5	2–4	0.07
Two interfaces						
VII	3	33, 33, 99	288, 288, 864	5	2–4	0.07
Dependence on h_0						
VIII	2	0, 33, 66	1, 1024, 1024	2.5	2–13	0.01
IX	2	0, 33, 66	1, 512, 512	5	2–14	0.01
X	2	0, 33, 66	1, 512, 512	6.5	2–12	0.01
XI	2	0, 33, 66	1, 512, 512	7.5	2–10	0.01

TABLE 2. Listing of all the simulations performed. Each simulation is referred to by a Roman numeral, shown in the left column. For each simulation we also list the values of the number of dimensions, domain sizes, number of grid points in the S-field, initial interface thicknesses (h_0), range of R_ρ simulated, and τ. All simulations are initialized with equal interface thicknesses for T and S.

dimensionless parameters above, it is also possible to define dimensionless domain sizes $\{L_x, L_y, L_z\}/h_T$.

2.3. *Comparison with geophysical observations and laboratory experiments*

The choice of dimensional scales used in the simulations is motivated by recent measurements that have been made in the thermohaline staircase of Lake Kivu by Schmid *et al.* (2010) and Sommer *et al.* (2013), as well as by limitations in computational resources. The range of these parameters and scales is given in table 1, showing that the DNS lies well within the range of that found in Lake Kivu.

A total of eleven simulations have been performed, and are summarized in table 2. In keeping with the analogy with run-down laboratory experiments of previous investigations that have used heat, salt, and other soluble components with various diffusivities (e.g. Turner *et al.* 1970; Shirtcliffe 1973; Newell 1984; Stamp *et al.* 1998), we have chosen four simulations in which τ is varied (simulations I–IV). The range of τ chosen is from the heat–salt value of 0.01 to the salt–sugar value of 0.33. By

varying τ we are able to gain insight into the processes that control the structure of the diffusive interface. In addition, we also take $\tau = 0.07$, and investigate the dependence of the results on the vertical and horizontal size of the domain (simulations V and VI), perform a simulation with two interfaces (simulation VII), and test the dependence on the initial interface thicknesses in a series of two-dimensional simulations at the heat–salt value of $\tau = 0.01$ (simulations VIII–XI).

2.4. *Capturing scalar mixing at low diffusivities*

In the classical Kolmogorov theory of turbulence, the length of the smallest eddies scales with the Kolmogorov length $L_K \equiv (\nu^3/\epsilon)^{1/4}$, where ϵ is the volume-averaged rate of dissipation of kinetic energy. In the spectral-method-based DNS of homogeneous flows, grid resolutions that are of the order of L_K are usually required for adequately capturing the dissipation of kinetic energy – though simulations using grid spacings up to $14L_K$ have been found sufficient (Moin & Mahesh 1998). However, when simulating scalar fields with molecular diffusivities that are smaller than ν (i.e. for $Pr > 1$ and $\tau < 1$) it is the scalar field with the smallest diffusivity that produces the smallest scales. In the simulations performed in this study, it is therefore the S-field that requires the greatest numerical resolution. According to the theory of scalar turbulence put forward by Batchelor (1959), the smallest scales are now determined by the Batchelor length $L_B = L_K\,(\tau/Pr)^{1/2}$, in the case of the S-field. It is important to keep in mind that L_B only denotes a single length within a continuous spectrum of turbulent length scales in which diffusion is acting to damp scalar gradients, and does not necessarily need to be resolved in DNS. Indeed, well-resolved DNS of stably stratified mixing layers have utilized grid spacings of $2.5L_B$ (Smyth & Moum 2000; Smyth, Moum & Caldwell 2001). In the present simulations, the resolution of the S-field had an even grid spacing, Δx, in each of the three dimensions, that always satisfied $\Delta x/L_B < 2$. The largest $\Delta x/L_B \approx 2$ ratio occurred in the three-dimensional $\tau = 0.01$ simulation (I) during the initial instability of the interface (discussed in § 3).

In addition to the $\Delta x/L_B$ ratio, we also monitor the background potential energy P_b of the scalar fields, defined by

$$P_b \equiv \frac{g}{L_z}\int_0^{L_z} \varphi_b z_b \,\mathrm{d}z_b, \tag{2.5}$$

where $\varphi_b(z_b)$ is the background scalar field obtained by re-sorting all the $\varphi(x, y, z)$ elements in the domain into a single (monotonic) one-dimensional profile. The z_b grid of φ_b has the length L_z, but with a total number of elements equal to that of the full three-dimensional domain (see Winters *et al.* 1995, for further details). Since the boundary conditions do not permit the flux of φ across them, P_b must be a monotonic function of t, expressing the fact that scalar mixing is an irreversible process. Our experience has shown that this is the most stringent criterion for adequately resolving turbulent scalar mixing with DNS. By monitoring $\mathrm{d}P_b/\mathrm{d}t$ we found that the resolution of the S-field in simulation I, with the oceanic heat–salt value of $\tau = 0.01$, was not sufficient at early times (i.e. $\mathrm{d}P_b/\mathrm{d}t$ was found to change sign). For this reason, the results of this simulation must be treated with caution, and we shall generally focus our study on the low-τ simulation II. However, results from all simulations will be used when discussing the dependence on τ, and in this case our conclusions from simulation I are supported by the higher-resolution two-dimensional simulations (VIII–XI) at $\tau = 0.01$.

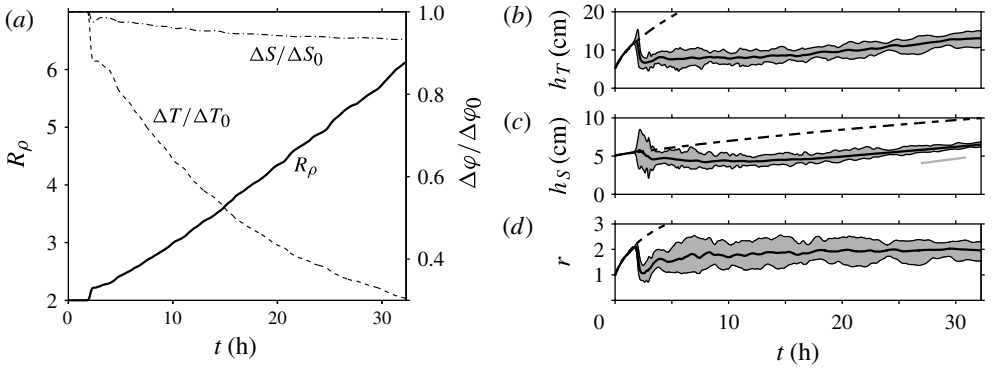

FIGURE 2. The time-dependent run-down of various quantities for simulation II ($\tau = 0.035$). (*a*) The decrease in the mixed-layer *TS* differences ΔT and ΔS (dashed and dash-dot lines, respectively), normalized by their initial values at $t = 0$, denoted by $\Delta\varphi_0$, as well as the ratio R_ρ. (*b–d*) The evolution of the interface thicknesses h_T, h_S, and the ratio r, respectively: the thick solid line represents the mean with the grey shading showing the 10th and 90th percentiles within the domain; the dashed line shows the hypothetical interface growth due to only molecular diffusion. The slope of the grey line in (*c*) indicates the rate of growth of the salinity interface by molecular diffusion at a thickness of 6 cm.

In simulation VIII, the initial breakdown of the thin interface at $\tau = 0.01$ resulted in very sharp *S*-gradients, and we were required to use an especially fine resolution in this case.

3. Time evolution

3.1. *General description*

It is beneficial to begin with an initial description of the time evolution of the diffusive interface. This is shown in figure 2 where the run-down of both the mixed-layer *TS* differences, as well as the interface thicknesses, are plotted together with the dimensionless ratios R_ρ and r, for simulation II ($\tau = 0.035$). In figure 2, and throughout this paper, we shall often use dimensional units (e.g. hours and cm). The reason for this is that since the dimensional parameters of the simulations are comparable to those found in relevant geophysical staircases, we believe that using dimensional values – as opposed to a time scale of $(\kappa_T/g^2)^{1/3}$, say – gives one more insight into these systems.

In all simulations, the *TS*-profiles are initiated, at $t = 0$ h, with the same interfacial thicknesses ($r = 1$), and $R_\rho = 2$. The linear stability analysis of Carpenter *et al.* (2012) has shown (for $\tau = 0.01$ and $Pr = 6$) that this corresponds to a stable configuration of T and S. However, as time increases, both interfaces grow in thickness by molecular diffusion at a rate that is proportional to $\kappa_\varphi^{1/2}$. Since $\kappa_T > \kappa_S$ the T-interface becomes thicker than the S-interface, and r increases (figure 2*b–d*). Owing to the gravitationally unstable configuration of T, this mismatch of interface thicknesses when $r > 1$ has the effect of producing regions of gravitationally unstable density stratification above and below the gravitationally stable central core (figure 3). The gravitationally unstable layers are generally referred to as the 'diffusive boundary layers', and when $r > 1$ the interface is said to display a 'double-boundary-layer' structure (Fernando 1989). The diffusive boundary layer, and how it is coupled to both the stable core of the interface

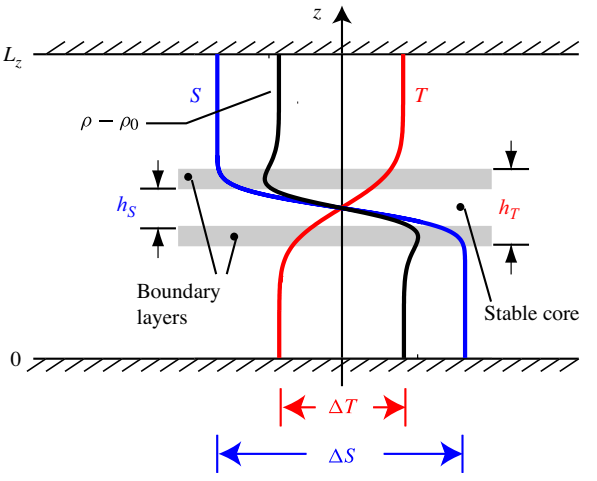

FIGURE 3. (Colour online) Illustration of the development of diffusive boundary layers due to the relatively thicker T-interface. The grey shaded regions highlight the location of the boundary layers and have a vertical height of $b = (h_T - h_S)/2$, which is to be used as a characteristic boundary layer length scale in § 6. Recall that both T and S are plotted in density units.

and the mixed layers, is a common basis for a number of phenomenological models of the fluxes across the diffusive interface (e.g. Linden & Shirtcliffe 1978; Newell 1984; Fernando 1989; Kelley 1990; Worster 2004).

Convection begins at $t \approx 2$ h when the gravitationally unstable boundary layers break away from the stable interface core. At this time h_T and h_S depart from growth by pure molecular diffusion (dashed curves in figure 2*b*,*c*), and experience a rapid thinning. There is a sharp increase in R_ρ as the boundary layer fluid is mixed into the upper and lower mixed layers (figure 2*a*). This time period, after the initial breakdown of the boundary layers, is the most energetic phase of the turbulence in the mixed layers. It displays elevated levels of the kinetic energy dissipation rate, and is therefore also the most difficult period to resolve numerically.

After the period of high turbulence following the initial breakdown of the boundary layers, the interfaces appear to slowly adjust to a preferred thickness ratio ($r \approx 2$ for simulation II). Figure 2 shows that while h_T is continuously increasing in t, h_S is initially eroded by the convective motions until $r \approx 2$ is reached. This apparent adjustment to a preferred value of r was observed in nearly all of the simulations performed, and can be seen in figure 4 for simulations I–IV. In each case, however, after the initial adjustment, r is still changing slowly in time. In § 6, we shall provide a possible explanation in terms of the interface stability.

3.2. *Dependence on initial conditions*

Worster (2004) has formulated an extension of the Linden & Shirtcliffe (1978) model of the diffusive interface that includes time dependence. The application of this model to laboratory experiments has found good agreement, and shows that the evolution of the diffusive interface is often dependent on the initial conditions. To test this dependence of the DNS we analyse a series of two-dimensional simulations (VIII–XI) at $\tau = 0.01$. Each simulation is initialized with a different interface thickness $h_0 = h_\varphi(t = 0)$, where we fix $h_T = h_S$ (i.e. $r = 1$) at $t = 0$. The evolution of h_T, h_S,

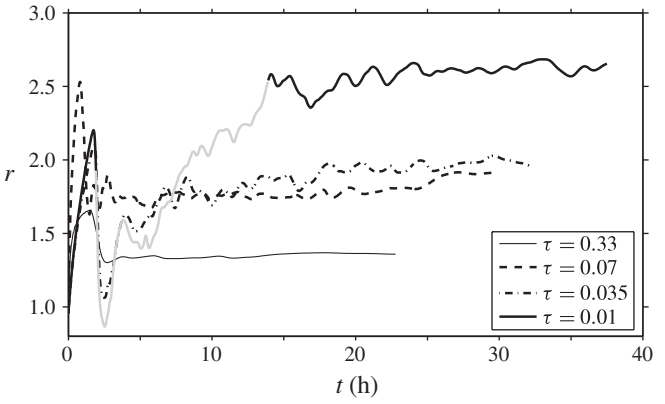

FIGURE 4. Time evolution of r for simulations I–IV at different τ. The grey colour of the $\tau = 0.01$ curve indicates the time over which the S-field was not completely well-resolved.

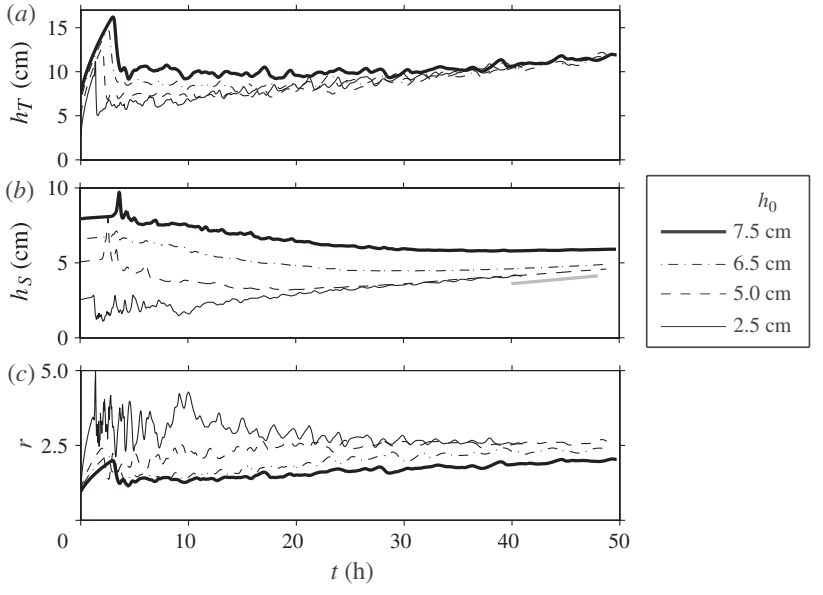

FIGURE 5. Time evolution of interface thicknesses (*a*) h_T, (*b*) h_S, and (*c*) their ratio r, for the sequence of two-dimensional simulations (VIII–XI) at $\tau = 0.01$ for various initial thicknesses h_0. The grey line in (*b*) indicates the rate of growth of h_S by molecular diffusion at a thickness of 5 cm.

and r in time is shown in figure 5. The evolution of $h_\varphi(t)$ is in general similar to that shown in figures 2 and 4. In each case, once convection begins h_S decreases as the salinity interface is initially eroded. This period of erosion becomes longer for each increase in the initial h_S value. For the largest initial $h_S = 7.5$ cm, the period of h_S growth has not yet begun by the end of the simulation. As in figure 4, each of the simulations in figure 5(*c*) appears to approach a relatively constant value of the interface thickness ratio. For the two simulations with $h_0 = 2.5$ and 5 cm (VIII,

IX), the final value of $r \approx 2.6$ is nearly identical with the value found from the three-dimensional simulation (I). However, the simulations at the thickest initial values of $h_0 = 6.5$ and 7.5 cm have not yet reached this approximately steady value of r.

A consistent run-down of the diffusive interface appears to be attained once the relatively constant value of r is reached. This is seen to be the case in each of the simulations (I–IV) in figure 4, as well as the $h_0 = 2.5$ and 5 cm simulations (VIII, IX) of figure 5. The run-down evolution of the diffusive interface once this state is reached may be understood by referring to the basic assumptions behind the model of Newell (1984), which can also be recovered from the more general formulation of Worster (2004). Initially formulated for the large-R_ρ region, with $R_\rho > \tau^{-1/2}$, Newell (1984) was able to predict reasonable estimates of interface thicknesses and fluxes based largely on the assumption that the S-interface growth is controlled by molecular diffusion. This has been found to be a good approximation to the time evolution of h_S for late times, once a constant r is reached. The expected rate of growth of h_S by molecular diffusion alone is indicated by the slope of the grey lines in figures 5(*b*) and 2(*c*), and is found to agree closely with the observed h_S increase. Since molecular diffusion causes smaller interfaces to grow faster than thicker interfaces, the $h_S(t)$ curves in figure 5(*b*) should all collapse onto a single curve at late times. This is seen to be nearly the case for three of the four simulations. Details of the Newell (1984) model and its implications for the heat fluxes will be discussed further in § 5.

4. Interface and boundary layer structure

4.1. *Phenomenological description*

In the previous section we showed that a persistent double-boundary-layer structure is present in all of the simulations. This can be seen in figure 1, and results in gravitationally unstable boundary layers above and below the stable interface core. This boundary layer is ultimately responsible for producing turbulence and mixing in the mixed layers, and a number of previous studies have proposed mechanisms to describe the coupling between the boundary layer and the mixed layer (Linden & Shirtcliffe 1978; Fernando 1989; Kelley 1990).

Kelley (1990) describes a model that is based on a large-scale circulation within the mixed layers. This circulation causes a highly sheared horizontal flow within the boundary layer, which forms thin sheet-like plumes that transport the boundary layer fluid vertically into the mixed layers. This description appears to be in good qualitative agreement with the simulations. Relatively thin plumes can be seen in figure 1, as well as in the density field plotted in figure 6(*c*), to be responsible for transporting boundary layer fluid into the mixed layers. To highlight the locations of the plumes in time we plot a scaled $2T/\Delta T(t)$ field taken at the vertical level $z = h_T(t) + L_z/2$, at the locations $y = 0$ and $x = 0$ in figures 6(*a*) and 6(*b*) respectively. This shows that the plumes are quasi-steady features with generally one plume being present in each layer. Note that although the plumes are persistent in time, there are always fluctuations in the size (inferred from the T anomaly present). These fluctuations appear to arise from the formation of new unstable plumes breaking away from the boundary layer, which are subsequently swept into the established plume sites by a large-scale circulation. This causes oscillations of the strength of the established plumes seen in figure 6(*a,b*). In addition to the fluctuations in plume strength, there are a number of shifts in the plume location.

The large-scale circulation can be seen from the two representative streamline patterns taken at different times and in different planes in figure 7, superimposed

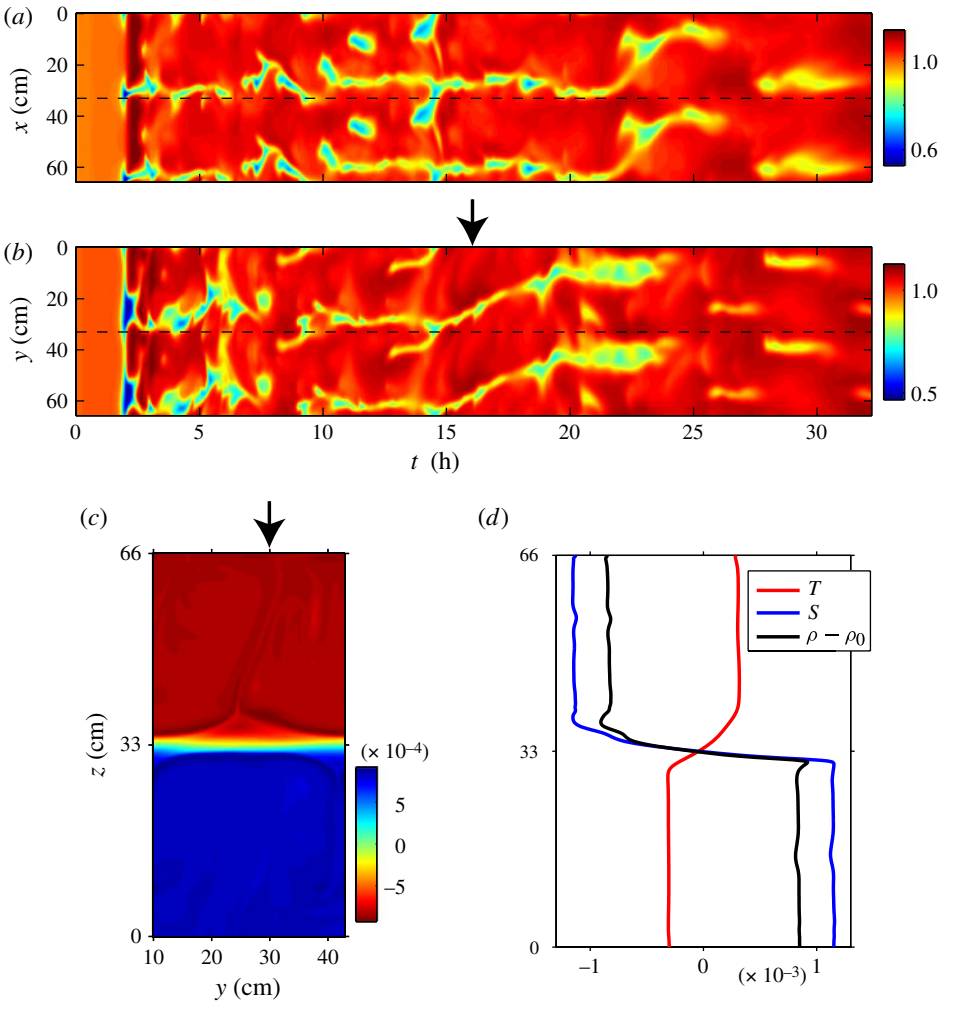

FIGURE 6. (*a*) Plot of $2T(x,t)/\Delta T$ for $y = 0$ cm and $z = h_T + L_z/2$ in simulation II showing the location of the plumes at low $2T/\Delta T$ values (recall that T is in density units) as a function of t. (*b*) As in (*a*) but in the plane $x = 0$ cm. In both (*a*) and (*b*) two domains have been included in the spatial dimension for clarity, with the true domain size indicated by the dashed line. The location of the arrow in (*b*) indicates the time at which the density field $\rho - \rho_0$ at $t = 16$ h and $x = 0$ cm, shown in (*c*) is taken. Representative examples of T-, S-, and $\rho - \rho_0$-profiles are shown in (*d*) from $y = 30$ cm (indicated by the arrow in *c*), $x = 0$ cm and $t = 16$ h.

on shaded plots of the vertical T-gradient. The streamlines show the presence of large-scale circulations in the mixed layers, with very little small-scale turbulent motions. The structure of the velocity field in the same two-dimensional slice as that shown in figure 1(*b*,*c*), is plotted in figure 7(*b*). At this time, a new plume is in the process of forming and breaking away from the lower boundary layer near $x \approx 28$ cm.

In contrast to the Kelley (1990) model of steady large-scale circulations driven by plumes from the boundary layers, Linden & Shirtcliffe (1978) present a model that is based on the growth of the boundary layer by diffusion, then a sudden

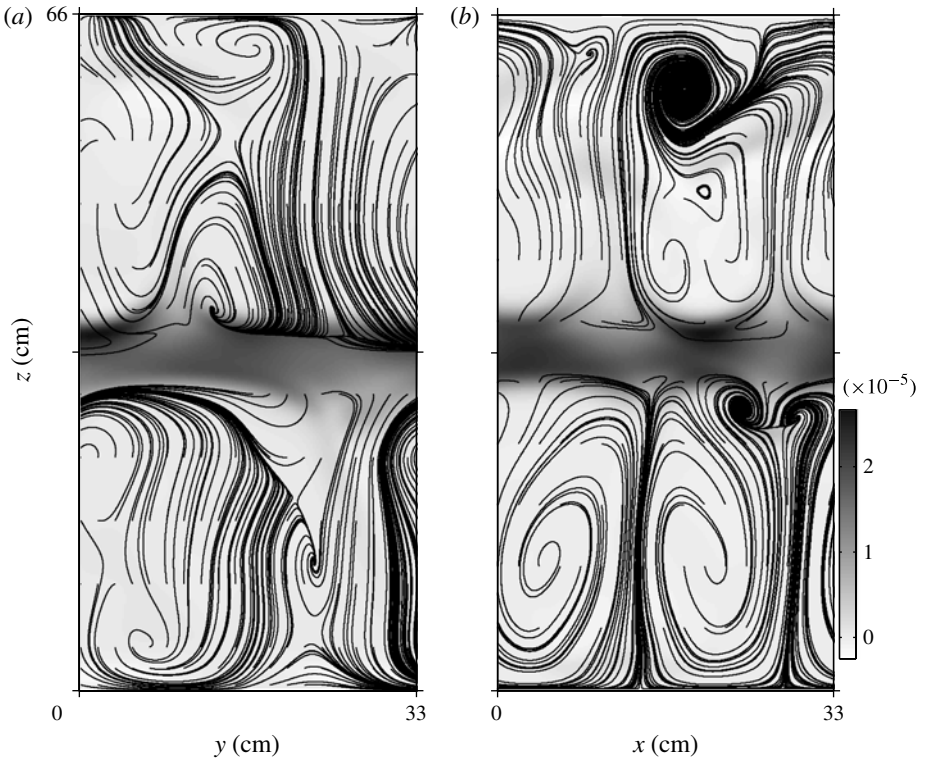

FIGURE 7. Streamlines superimposed on a grey colour plot of the vertical T-gradient $\partial T/\partial z$ in units of kg m^{-4}. The plots are taken at the times (*a*) $t = 16$ h at $x = 0$ cm, and (*b*) $t = 11.4$ h at $y = 0$ cm; (*a*) and (*b*) correspond to the times and locations of the density plots in figure 6(*c*), and figure 1, respectively.

breaking away of this unstable layer through a convective instability. The present simulations display elements of both theories, with a persistent unstable boundary layer present (figure 6*c,d*) that feeds quasi-steady plumes in support of the Kelley (1990) description, as well as periodically fluctuating flow and plume strength due to the formation of instabilities in the boundary layer also leading to shifts in the large-scale circulation in support of Linden & Shirtcliffe (1978). It should be noted that since the convection usually consists of only a single cell the small domain size is likely to be exerting an influence on the flow. However, no significant changes were found in simulations V and VI where the domain size was increased.

4.2. *Vertical structure of the interface and boundary layers*

Despite the fluctuations and shifts of the large-scale circulation, we may obtain a meaningful picture of the mean velocity structure in the vicinity of the interface if we scale the vertical z coordinate by the half-width of the T-interface thickness, i.e. by defining the dimensionless vertical coordinate

$$\zeta(t) \equiv \frac{2(z - L_z/2)}{h_T(t)}. \tag{4.1}$$

Once plotted as a function of ζ, and normalized by the volume average to remove the time-dependent amplitude, the root-mean-squared (r.m.s.) vertical velocity field shows

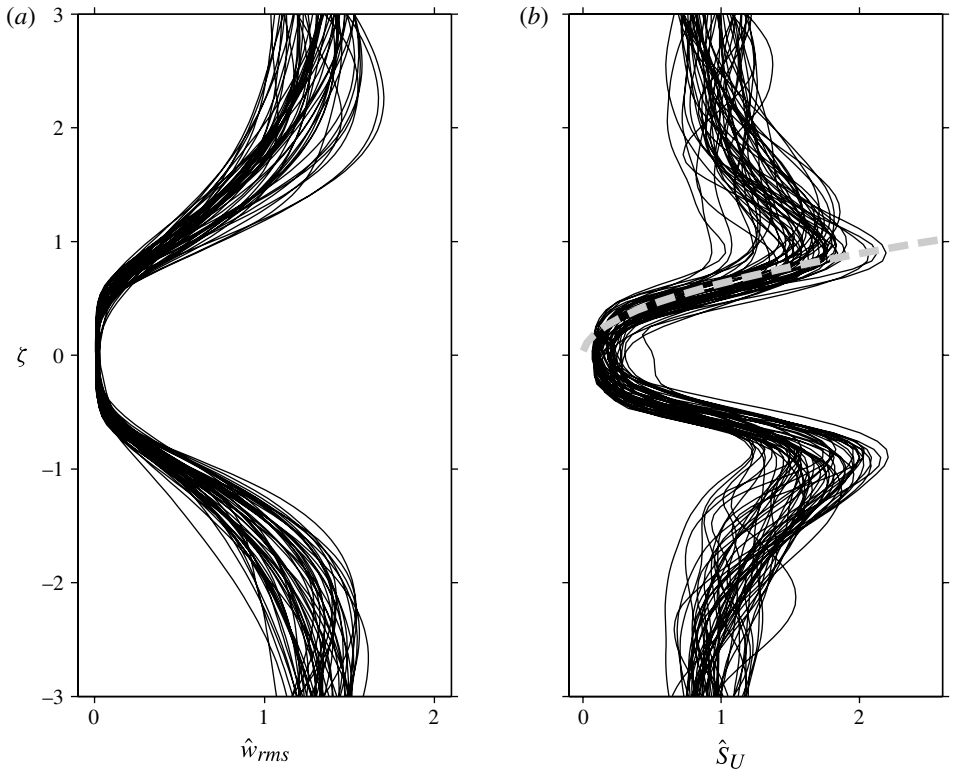

FIGURE 8. Profiles of (*a*) $\hat{w}_{rms}(\zeta)$ and (*b*) $\hat{S}_U(\zeta)$ every 0.5 h from $t = 5.8$ h to the end of the simulation at $t = 32$ h ($2.5 < R_\rho < 6.1$). The grey dashed line in (*b*) shows an $\hat{S}_U \propto \zeta^2$ dependence for comparison.

reasonable collapse to a similar form for small ζ (figure 8*a*). Mathematically, this can be written as

$$\hat{w}_{rms}(\zeta, t) \equiv \sqrt{\frac{\langle w^2 \rangle_{xy}}{\langle w^2 \rangle_{xyz}}}, \tag{4.2}$$

where we use angled brackets to denote averaging over the variable X as $\langle\rangle_X$. This averaging reduces the (spatial) variability between profiles at various t. The averaged profiles are plotted every half-hour in figure 8, from $t = 5.8$ to 32 h and $R_\rho = 2.5$ to 6.1, after the initial phase of intense turbulence. It can be seen that the vertical velocity vanishes within the interface, indicating that mixed-layer turbulence is not able to penetrate the stable stratification of the core. This has significant implications for the fluxes of T and S that will be discussed in the following section.

Also, shown in figure 8(*b*) is the scaled mean horizontal shear defined by

$$\hat{S}_U(\zeta, t) \equiv \frac{\langle S_U \rangle_{xy}}{\langle S_U \rangle_{xyz}} \quad \text{with} \quad S_U \equiv \sqrt{\left(\frac{\partial u}{\partial z}\right)^2 + \left(\frac{\partial v}{\partial z}\right)^2}. \tag{4.3}$$

An elevated shear can be seen within the boundary layers, which diminishes as the stable core of the interface is approached. In keeping with our phenomenological

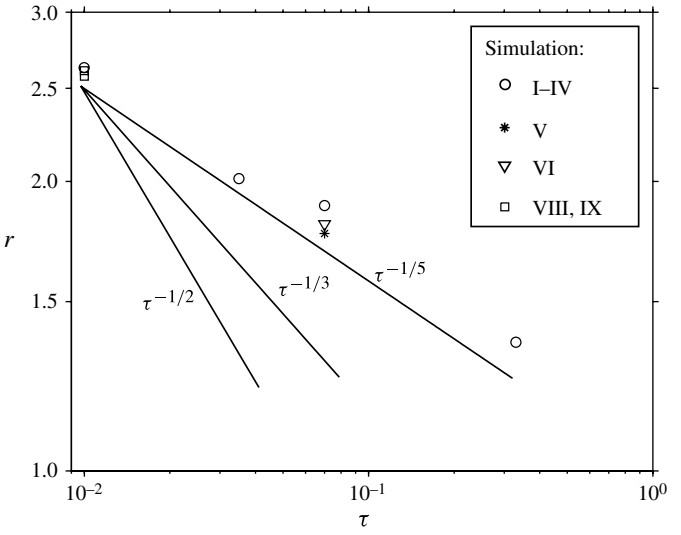

FIGURE 9. Scaling of r with τ for three-dimensional simulations (I–VI) and the two-dimensional simulations (VIII, IX), together with the slopes of the $\tau^{-1/2}$, $\tau^{-1/3}$, and $\tau^{-1/5}$ models for comparison. The values of r were determined by averaging the last 10 h of the mean $r(t)$ for each simulation.

description, the source for the elevated shear in the boundary layers appears to result from the boundary layer fluid being drawn horizontally towards the plume sites. This observation provides some support for the Kelley (1990) model, which assumes that all of the kinetic energy dissipation occurs in the horizontally sheared boundary layers. However, we also observe significant shear (and hence dissipation) to be present in the mixed layers.

4.3. *Scaling of the interface thickness ratio*

Although the simulations do appear to adjust to a state in which r is slowly changing in time, it is nonetheless instructive to compare the approximate scaling of r with τ to gain further insight into the double-boundary-layer structure. Figure 9 shows a log–log plot comparing the four simulations with different τ, along with the two $\tau = 0.07$ simulations (V and VI) where the domain size was varied, and the two-dimensional simulations (VIII and IX) with $\tau = 0.01$. The r values plotted were obtained by averaging over the final 10 h of each simulation (see figure 4 for an indication of this averaging time). A definite dependence of r on τ is observed. As one would expect intuitively, smaller values of τ – and therefore a greater difference in the T and S molecular diffusion 'speeds' – lead to larger values of r, i.e. greater differences between the relative interface thicknesses.

It is interesting to compare the observed scaling of r with τ to two simple models of the diffusive interface. In each model we assume that interfaces grow by molecular diffusion according to

$$h_\varphi \propto (\kappa_\varphi t)^{1/2}. \tag{4.4}$$

In the first model we take the time scale, t_*, over which the convection process removes the boundary layer fluid to be equal for both T and S. Substituting $t = t_*$ into (4.4) the ratio of interface thicknesses then gives the scaling $r \sim \tau^{-1/2}$ (figure 9).

This scaling was suggested previously by Fernando (1989). Note that this scaling also assumes that sufficient time has elapsed between entrainment events of the boundary layer fluid.

The second model builds on the interpretation of Kelley (1990), which was qualitatively found to match our observations, as discussed above. Since the boundary layer fluid is acted on by a large-scale circulation that sweeps it towards the plumes, and because we find that a shear is present across the boundary layers, we should expect that the time scale for diffusion of the T- and S-interfaces is different. The shear enhances the lateral transport of T relative to S, since the thicker T-interface finds itself in regions of larger velocity. The time scale for growth of each interface can then be expressed as $t_{*\varphi} \sim \ell/S_U h_\varphi$, where ℓ is the distance between plumes, and S_U is a measure of the velocity shear. In the case of a constant shear, we substitute $t_{*\varphi}$ into (4.4), taking the ratio, and solving for r yields a $r \sim \tau^{-1/3}$ scaling. This scaling has been proposed to describe the relative thicknesses of the velocity and thermal boundary layers in thermal convection close to a solid no-slip boundary (Grossman & Lohse 2000).

Although taking account of the shear across the interfaces leads to an estimate that is closer to the observations in figure 9, the profiles in figure 8(*b*) show that the shear across the interface region (from $-1 < \zeta < 1$) is not constant. We therefore propose a more general time scale that accounts for a depth dependence of shear given by

$$t_* = \frac{\ell}{\displaystyle\int_0^1 S_U(\zeta)\,\mathrm{d}\zeta} \tag{4.5}$$

with the denominator representing an effective velocity scale for the advection of the interfaces (by symmetry only the upper half need be considered). Choosing a form that is more representative for the shear $S_U \propto \zeta^2$, as shown in figure 8(*b*), leads to a scaling that is closer to the observations of $r \sim \tau^{-1/5}$. Note that any power-law relationship could be used, i.e. $S_U \propto \zeta^n$, and would lead to a scaling of $r \sim \tau^{-1/(n+3)}$. However, despite the obvious improvements when a variable shear profile is used, we do not have an adequate number of simulations to accurately test for the best scaling.

It should also be noted that as $\tau \to 1$ the interface thicknesses should be increasingly dominated by molecular diffusion, rather than the DD convection process, and we must have $r \to 1$, as appears to be the case. The value of r is also found to vary weakly with the domain sizes L_x and L_z, indicating that the domain size may exert an influence on the properties of the boundary layers. Simulations in larger domains with many large-scale convection cells may reduce this scatter.

5. Heat and salt fluxes

5.1. *Are the fluxes through the interface molecular?*

Of primary importance in the study of DD convection are the fluxes, denoted by F_φ, of T and S across the interface. Furthermore, it is possible to compute these quantities very precisely from DNS. The method that we use is based on the framework of Winters *et al.* (1995) and Winters & D'Asaro (1996). Every grid point in the domain from the φ scalar field is assembled and sorted to form a single monotonic background profile $\varphi(z_b)$, where $z_b(\varphi_0)$ denotes the background level of the φ_0 scalar value. Since the boundary conditions permit no flux of φ across them, the total 'φ-mass' within the

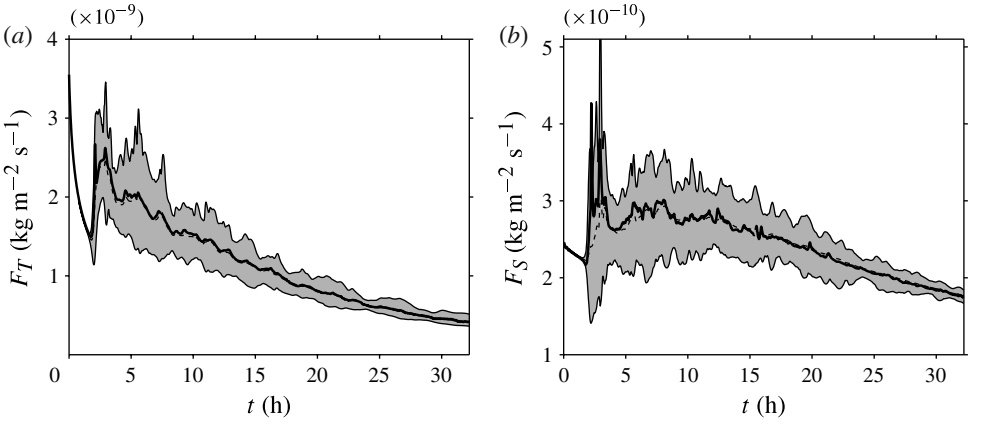

FIGURE 10. Measures of the fluxes of (*a*) T and (*b*) S across the diffusive interface for simulation II ($\tau = 0.035$). The thick solid line denotes the total flux F_φ, while the thick dashed line indicates the average molecular flux F_φ^{mol}. Throughout most of the simulation $F_\varphi \approx F_\varphi^{mol}$, and the dashed curve is difficult to distinguish from the solid. The grey shading gives the 10th and 90th percentiles of F_φ^{mol} within the domain.

domain must be constant, i.e.

$$\int_V \varphi(x, y, z, t)\,\mathrm{d}V = \int_0^{Lz} \varphi(z_b)\,\mathrm{d}z_b = \text{const.}, \tag{5.1}$$

where V is the domain volume. The φ-flux, F_φ, through the φ_0-surface, is then easily computed by the total change in storage below (or above, depending on the sorting procedure) the level $z_b(\varphi_0)$, given by

$$F_\varphi = \frac{\mathrm{d}}{\mathrm{d}t} \int_0^{z_b(\varphi_0)} \varphi(z_b)\,\mathrm{d}z_b. \tag{5.2}$$

Choosing φ_0 to be the central T and S scalar values within the interface (i.e. $T_0 = \Delta T/2$ and $S_0 = \Delta S/2$) leads to the determination of the interfacial TS-fluxes. These are plotted as a time series for simulation II ($\tau = 0.035$) with the thick solid lines in figure 10.

In addition to the total flux F_φ across the diffusive interface, we also plot what we will refer to as the 'molecular' flux, F_φ^{mol}. This is defined mathematically by

$$F_\varphi^{mol} \equiv \kappa_\varphi \left.\frac{\partial \varphi}{\partial z}\right|_{\varphi_0} = \kappa_\varphi \frac{\Delta \varphi}{h_\varphi}, \tag{5.3}$$

where the φ_0 subscript indicates that the derivative is evaluated at the z where $\varphi = \varphi_0$, and the second equality follows from the definition of h_φ in (2.3). Physically, F_φ^{mol} is the vertical φ-flux at each horizontal location of the interface, assuming that the flux is purely molecular. In general, F_φ^{mol} need not be a single-valued function of (x, y) since the φ_0-surface could fold over itself; however, this was not found to be the case for any of the simulations. Both the average value of F_φ^{mol}, as well as the 10th and 90th percentiles found within the domain, are plotted in figure 10. This figure shows that, in general, the T- and S-fluxes are equal to their molecular values. An exception is the phase of intense turbulence from $t = 2$ to 4 h where F_S is in excess of F_S^{mol} by 10 %. A

similar spike occurs in F_T at $t \approx 2$ h, but is of very limited duration. For the remainder of the simulation $F_\varphi = F_\varphi^{mol}$ to within 5 %. It should be noted that a correction has been applied to F_φ^{mol} of 1.1 % in order to account for the averaging procedure when calculating the gradients in the interface (see § 2.2).

In general, the enhanced transport of scalar quantities that is associated with turbulent mixing (across some isoscalar surface) is accomplished by: (i) a sharpening of gradients; and (ii) an increased area of the isoscalar surface. The close agreement of F_φ and F_φ^{mol} shows that the enhanced transport of T and S at a diffusive interface is caused almost entirely by (i). This can be seen by noting that the total flux across any φ-surface for a turbulent flow is given at each point on the surface by the normal component of the diffusive flux, i.e. $\kappa_\varphi \nabla\varphi \cdot \hat{\boldsymbol{n}}$, where $\hat{\boldsymbol{n}}$ is the unit normal vector to the surface (Winters & D'Asaro 1996). Therefore, for a completely flat and horizontal φ-surface, the total flux is given entirely by its vertical component $\kappa_\varphi \nabla\varphi \cdot \hat{\boldsymbol{n}} = \kappa_\varphi \partial\varphi/\partial z$. This was found to be the case in all of the simulations performed, and is in agreement with the vanishing of the r.m.s. vertical velocity within the interface (figure 7*b*).

The formulation of many phenomenological models of the diffusive interface from previous studies has been based on the assumption of molecular fluxes through the interface core (Linden & Shirtcliffe 1978; Newell 1984; Kelley 1990). Furthermore, the field observations of Padman & Dillon (1987) and Timmermans *et al.* (2008) have shown a close agreement between F_T^{mol} and the F_T predicted by different laboratory-based flux laws. However, we are not aware of any study that has definitively shown the fluxes to be molecular, with the exception of the experiments of Shirtcliffe (1973) using a salt–sugar interface ($\tau \approx 0.33$).

5.2. *Comparison with flux laws*

The ability to calculate precise fluxes in the DNS allows a comparison with flux laws suggested by previous researchers. Figure 11(*a*) shows F_T plotted as a function of R_ρ for simulations I–IV. It has become customary to normalize F_T by the standard 4/3 flux law that is used in the case of single-component convection through a solid plane boundary (e.g. Turner 1973; Linden 2000), which is given in units of kg m^{-2} s^{-1} by

$$F_T^{SP} = \lambda^{SP} \kappa_T \left(\frac{g}{\rho_0 \nu \kappa_T} \right)^{1/3} (\Delta T)^{4/3}, \tag{5.4}$$

where λ^{SP} is a coefficient taken as 0.085. In this dimensionless form, a horizontal line on figure 11 would indicate that F_T is given by a 4/3 flux law with $F_T \propto \Delta T^{4/3}$. This form for the T-flux was first suggested by Turner (1965); however, he found that F_T was dependent on R_ρ, showing decreasing F_T (and F_T/F_T^{SP}) as R_ρ increases. In the case of the $\tau = 0.01$ simulation (I) we observe no strong dependence on R_ρ (figure 11). In all other simulations a decreasing F_T is observed with increasing R_ρ.

The flux laws of Kelley (1990) and Linden & Shirtcliffe (1978) generally show lower predicted fluxes than that observed in the simulations, with a stronger dependence on R_ρ. Note that the Kelley (1990) parameterization is only valid for oceanic values of $\tau \approx 0.01$ and $Pr \approx 7$, whereas the Linden & Shirtcliffe (1978) parameterization is valid for a range of τ and Pr, as long as the condition $2 < R_\rho < \tau^{-1/2}$ is met. We may therefore compare the Linden & Shirtcliffe (1978) predictions to all but the $\tau = 0.33$ simulation.

The behaviour of F_T once the $r \approx$ constant run-down state is reached can be understood by appealing to the model proposed by Newell (1984). This model is based on the following four assumptions describing the run-down of the interface.

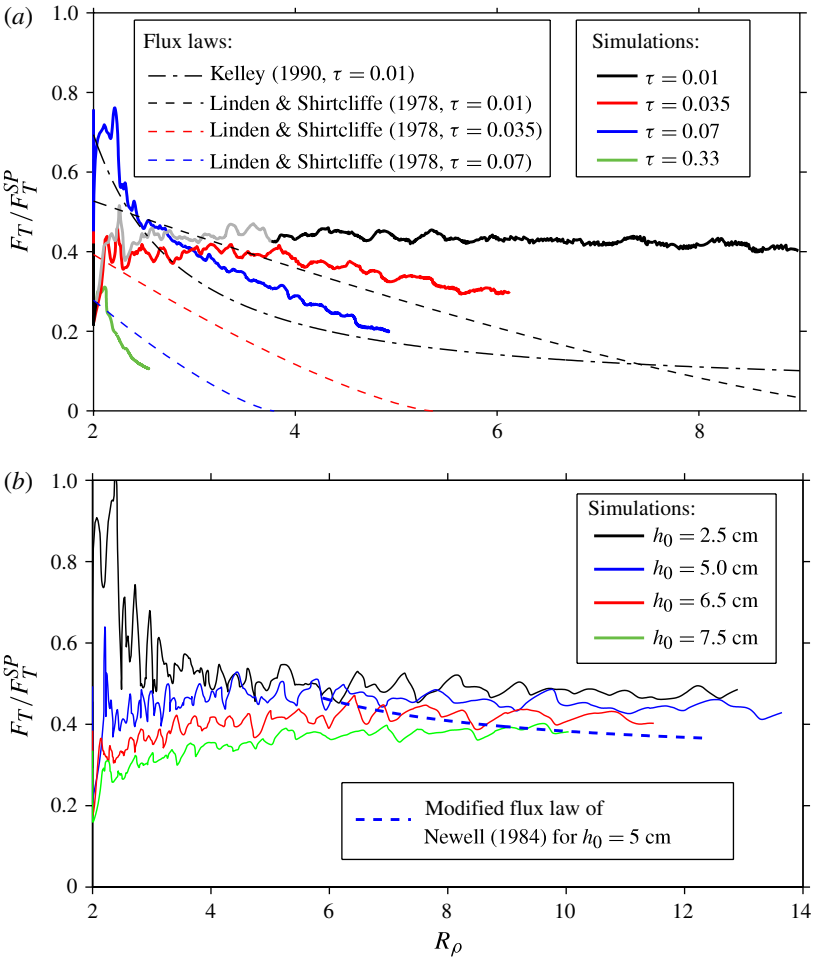

FIGURE 11. The dimensionless T-flux F_T/F_T^{SP} as a function of R_ρ for (a) simulations I–IV, and (b) the two-dimensional simulations (VIII–XI). Also shown in (a) are the predictions of the flux laws developed by Kelley (1990) for $\tau = 0.01$, and Linden & Shirtcliffe (1978) for $\tau = 0.01, 0.035, 0.07$. The grey region of the $\tau = 0.01$ curve indicates the period over which the S-field is not completely well-resolved.

(i) The fluxes through the interface are molecular, giving

$$F_T = \kappa_T \Delta T / h_T. \tag{5.5}$$

(ii) The S-interface evolution is determined by molecular diffusion, which, assuming an error function profile is given by

$$h_S(t) = 2\,[\pi \kappa_S (t + t_0)]^{1/2}, \tag{5.6}$$

where t_0 is a time shift used to recover an initial h_S condition.

(iii) The F_T through the interface is used entirely to heat the mixed layer, or in other words, the heat required to increase h_T is negligible. A heat balance then leads to

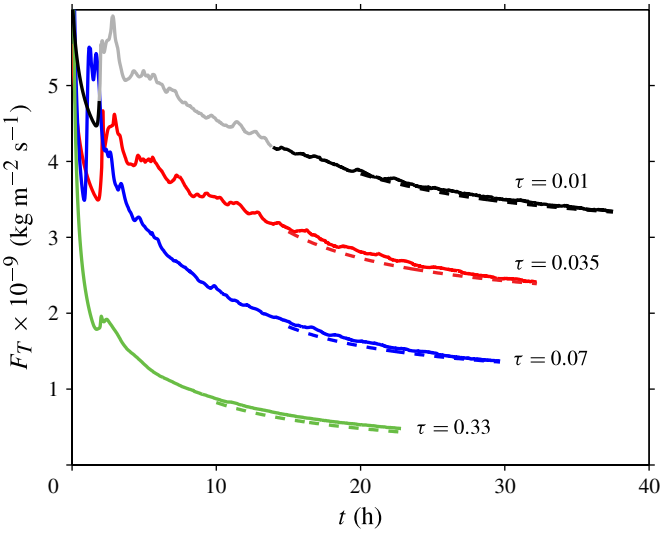

FIGURE 12. (Colour online) Comparison of F_T for simulations I–IV (solid lines) with the predictions of Newell's (1984) model (dashed). Each curve has been successively offset by 10^{-9} kg m^{-2} s^{-1} for clarity.

the relationship

$$\frac{\mathrm{d}\Delta T}{\mathrm{d}t} = -\frac{4}{L_z} F_T. \tag{5.7}$$

Note that we have assumed that the mixed layer is a constant thickness of $L_z/2$ rather than expressing it as a function of h_T.

(iv) A final assumption that is made by Newell (1984) based on measurements taken from laboratory experiments is that the T- and S-interfaces have the same thickness, i.e. $r = 1$. Our simulations show that the thickness ratio is a function of τ, and so we shall modify Newell's model with the fourth condition

$$\frac{\mathrm{d}h_T}{\mathrm{d}t} = r_0 \frac{\mathrm{d}h_S}{\mathrm{d}t}, \tag{5.8}$$

where r_0 is the approximately constant observed value of r.

Equations (5.5)–(5.8) describe an initial-value problem for a first-order ordinary differential equation that we can solve for $F_T(t)$, as well as other parameters such as $\Delta T(t)$ and $h_T(t)$. The resulting predictions for the T-flux are shown for simulations I–IV in figure 12, and are found to provide a good prediction of F_T once a constant r is reached. This modified Newell (1984) prediction is also shown in the F_T/F_T^{SP} versus R_ρ plot in figure 11(*b*), and predicts only a very gradual decrease in the normalized F_T as is observed in the simulations.

The results discussed above suggest the following interpretation of the run-down evolution of the diffusive interface. Turbulent motions within the mixed layers are unable to penetrate the strong stratification of the interface, and the resulting fluxes of T and S are described by a molecular flux law through the interface core. Owing to this lack of entrainment from the core, the increase of the S-interface thickness is determined by molecular diffusion. The shear that occurs within the boundary layers,

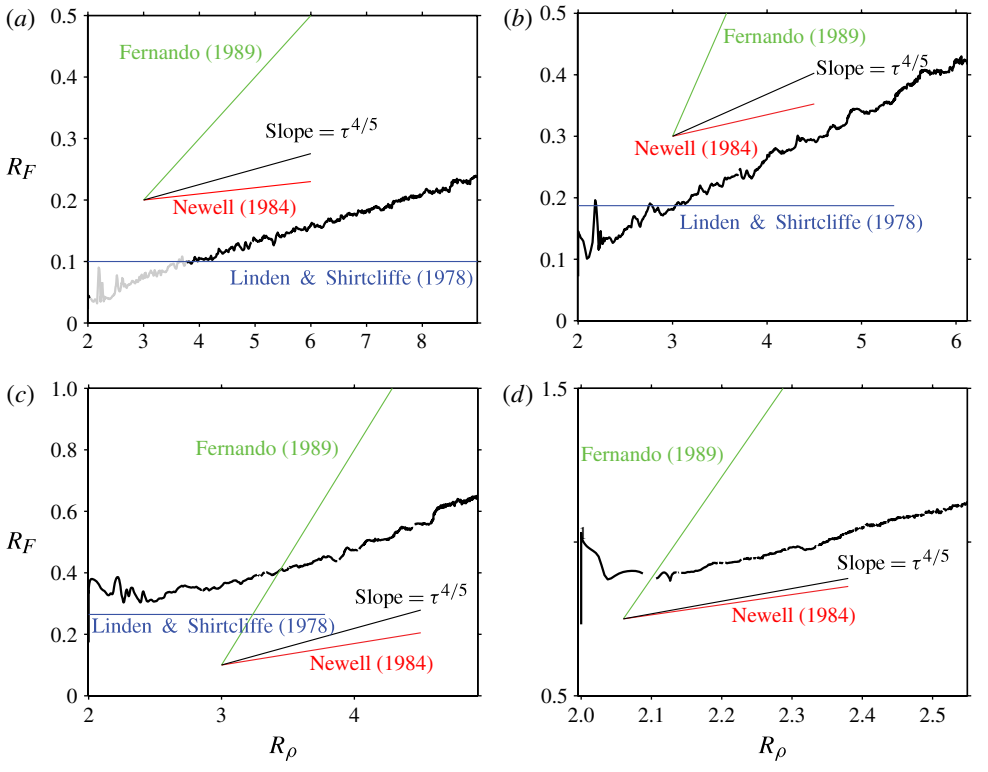

FIGURE 13. (Colour online) The flux ratio, R_F, plotted against R_ρ for simulations I–IV in which τ is varied: (*a*) $\tau = 0.01$; (*b*) 0.035; (*c*) 0.07; (*d*) 0.33. A comparison is made in each case with the slope predicted by the Newell (1984) and Fernando (1989) models. The Linden & Shirtcliffe (1978) prediction is for a constant $R_F = \tau^{1/2}$ for $R_\rho < \tau^{-1/2}$, and is therefore only shown in this region.

that is set up by the large-scale circulation, is then responsible for determining the T-interface thickness, and hence the T-flux. Owing to the slow growth of the S-interface in the low-τ simulations, we should expect the T-flux to follow a $\Delta T^{4/3}$ dependence, as seen by the weak R_ρ dependence of the curves in figure 11. This can be explained physically by the fact that a slowly diffusing and stable S-interface without significant entrainment acts similarly to a solid conducting plane. In this limiting case we should have an $F_T \sim \Delta T^{4/3}$ scaling, and a purely horizontal trajectory in figure 11.

5.3. *Coupled TS-fluxes: the flux ratio*

The observation of molecular fluxes through the interface has implications for the coupled transports of T and S. This is expressed by the flux ratio, defined as

$$R_F \equiv F_S/F_T. \tag{5.9}$$

It is customary to consider R_F to be a function of R_ρ for a given τ and Pr, and we have plotted this for simulations I–IV in figure 13.

In all cases, we observe an overall increasing R_F with R_ρ. The slope of these curves can be easily explained considering that: (i) the fluxes through the interface are molecular; and (ii) a relatively constant interface thickness ratio r, is observed. Writing

Study	R_F parameterization	Method
Turner (1965)	$R_F = 0.15$	Bottom-heated experiments using heat and salt ($\tau^{1/2} = 0.11$)
Shirtcliffe (1973)	$R_F = \tau^{1/2}$	Run-down experiments using salt and sugar
Linden & Shirtcliffe (1978)	$R_F = \tau^{1/2}$	Theoretical model
Takao & Narusawa (1980)	$R_F = 0.039\tau^{-1/3}$	Bottom-heated experiments using heat and various salts
Newell (1984)	$R_F = \tau R_\rho$	Run-down and bottom-heated experiments (heat–salt)
Fernando (1989)	$R_F = \tau^{1/2} R_\rho$	Bottom-heated experiments (heat–salt)
Stamp *et al.* (1998)	$R_F = \tau^{1/2}$	Run-down experiments (salt–sugar)

TABLE 3. Parameterizations suggested or found in previous studies. The vertical boundary conditions for the laboratory experiments are either of the run-down type, with no flux of T or S, or bottom-heated with a flux of T at the bottom boundary. In each study the R_F parameterization applies when R_ρ is not too small, which is generally for $R_\rho \gtrsim 2$.

the flux as $F_\varphi = \kappa_\varphi \Delta\varphi / h_\varphi$, and taking the ratio leads to

$$R_F = \tau r R_\rho. \tag{5.10}$$

Therefore, we expect the R_F versus R_ρ curve to be an approximately straight line with slope τr. Using the scaling of $r \sim \tau^{-1/5}$, we predict a slope of $\tau^{4/5}$ for the curves, and this prediction is shown in figure 13.

A number of previous studies have made predictions for the R_F versus R_ρ relationship that we can use as a reference to compare with. These parameterizations and the methods used to develop them are listed in table 3. Newell (1984) proposed a similar model to that above, in which he took $r = 1$ based on profiles measured from laboratory experiments. However, his experiments were generally carried out in the so-called large-R_ρ regime, where $R_\rho > \tau^{-1/2}$. In another model of the diffusive interface, Fernando (1989) argues that the interface thicknesses are determined by a competition between growth by diffusion, and entrainment by turbulent convective motions. He assumes that the time scale between successive turbulent entrainment events is long enough that $r = \tau^{-1/2}$. The R_F curve should therefore follow a much steeper slope than that of Newell (1984), as shown in figure 13. However, our lack of turbulent motion in the interface (see figures 7*b* and 10) suggests that the Fernando (1989) model is not valid for our simulations, and this may be due to the different boundary conditions used in the bottom-heated experiments of Fernando (1989). Yet another model of the diffusive interface, due to Linden & Shirtcliffe (1978), supposes that the interfacial fluxes are determined by the periodic breaking away of boundary layer fluid once a critical boundary layer Rayleigh number is reached. By assuming that T and S are diffused into the boundary layer over equivalent time scales, and that the entire boundary layer breaks away from the interface, they predict that $R_F = \tau^{1/2}$, independent of R_ρ. The Linden & Shirtcliffe (1978) model result was first found experimentally by Shirtcliffe (1973), in reasonable agreement with the experiments of Turner (1965), and is only expected to apply for the intermediate-R_ρ range of $2 \lesssim R_\rho < \tau^{-1/2}$, as plotted in figure 13.

Figure 13 clearly shows that the simulations are best described by the $R_F = \tau r R_\rho$ relation in (5.10) when the observed scaling of $r \sim \tau^{-1/5}$ is used. Although this finding is in agreement with the model presented in Newell (1984) when r is parameterized appropriately, it does not agree with the many studies showing a $R_F =$ constant relationship (see table 3). From our simulations it would seem that the R_ρ dependence of R_F is a general feature of the run-down configuration; however, we have no satisfactory explanation for the discrepancy with the experiments of Shirtcliffe (1973) and Stamp *et al.* (1998) showing a constant R_F.

6. Boundary layer stability

We have thus far observed that the diffusive interface naturally evolves to a double-boundary-layer structure with $r > 1$. Turbulent motions are suppressed by the stable interface core, and the interfacial fluxes are governed by molecular transport. We see, therefore, that it is natural for the diffusive interface to support a gravitationally unstable boundary layer. The question arises, however, as to just how unstable this layer becomes? We shall now address this question by appealing to the ideas presented in Linden & Shirtcliffe (1978), and to recent results utilizing a linear stability analysis by Carpenter *et al.* (2012).

Linden & Shirtcliffe (1978) proposed that the diffusive growth of the interfaces in time is limited by the gravitationally unstable boundary layer becoming hydrodynamically unstable, i.e. evolving to a state in which small perturbations will grow continuously in time. In accordance with the study of single-component convection by Howard (1964), they assumed that a breakdown of the boundary layer would be triggered once a critical boundary layer Rayleigh number $Ra_{bl,cr} \approx 10^3$ is exceeded. Ra_{bl} is defined by

$$Ra_{bl} \equiv \frac{g\delta\rho b^3}{\rho_0 \nu \kappa_T}, \tag{6.1}$$

where b is a representative length scale of the boundary layer (see figure 3) given by $b \equiv (h_T - h_S)/2$, and $\delta\rho$ is a representative boundary layer density scale, defined through the relation

$$\delta\rho\, b \equiv \int_{z_{bl}}^{L_z} [\Delta\rho/2 - |\bar{\rho}(z) - \rho_0|]\, \mathrm{d}z, \tag{6.2}$$

where $\Delta\rho = \Delta S - \Delta T$, $\bar{\rho}(z) = \langle\rho\rangle_{xy}$ is an average density profile, and z_{bl} is determined from $|\bar{\rho}(z_{bl}) - \rho_0| = \Delta\rho/2$. This choice of z_{bl} ensures that the integration in (6.2) is over the total gravitationally unstable density anomaly in the upper boundary layer. In other words, z_{bl} is chosen such that all the fluid in the upper boundary layer that is lighter than the mixed layer above is included in the integration (see Linden & Shirtcliffe 1978). Since a symmetry of the upper and lower boundary layers is assumed, the same reasoning applies below the interface. In practice, we assume an error-function profile for T and S with the same h_φ and $\Delta\varphi$ as measured, which allows us to write Ra_{bl} as a function of R_ρ, r, and Ra_I, as long as L_z/h_T is not too small (see Carpenter *et al.* 2012, for further details).

The Ra_{bl} condition of Linden & Shirtcliffe (1978) represents a plausible control on the growth of the boundary layer, and has received some tentative support from field observations (Padman & Dillon 1989; Sanchez & Roget 2007), although these observations lack sufficient knowledge of the S-field. It is possible to determine $Ra_{bl}(t)$ in the simulations, and this is shown in figure 14. First, it can be seen that much larger

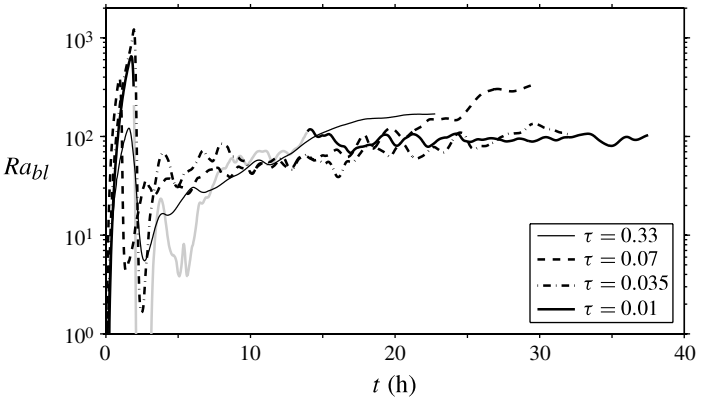

FIGURE 14. Ra_{bl} of the diffusive interface in time for simulations I–IV. The grey portion of the $\tau = 0.01$ curve denotes the period of the simulation that was not well-resolved.

Ra_{bl} are obtained when the diffusive interface grows from the quiet and stable initial condition at early times, than once the convection process has begun. If there was a true Ra_{bl} that represented an upper limit on the growth of the boundary layers, then we should expect to see the curves in figure 14 saturate at some level. Instead, for each simulation we see that there is a time dependence of Ra_{bl}. This time dependence is not very strong once a quasi-steady run-down of the interface has begun. Figure 14 does show that for the growing and convecting diffusive interface, an order-of-magnitude estimate of boundary layer conditions can be obtained with $Ra_{bl} = O(10^2)$, an order of magnitude lower than previously assumed.

The relatively constant values of Ra_{bl} attained in the simulations also support our observation that the boundary layer fluid is removed principally by quasi-steady large-scale motions in the mixed layers. If the periodic breakdown and subsequent growth of the boundary layers to an unstable state was occurring, then we should expect to see large fluctuations in the Ra_{bl} curves.

In the recent study of Carpenter *et al.* (2012), the linear stability of the diffusive interface was examined in detail. For the oceanographically relevant parameters of $\tau = 0.01$ and $Pr = 6$, instability was found to result from a convective-type mode in the gravitationally unstable boundary layers, confirming some of the basic assumptions of Linden & Shirtcliffe (1978). The stability analysis relies on the assumption of a frozen-in-time background state, and predicts that instability occurs for Ra_{bl} as low as 10. However, when the predictions of the stability analysis were tested using a two-dimensional DNS of the interface, it was found that the time dependence of the background state (which is diffusing in time) was important in determining the conditions at the point of boundary layer breakdown. The value of $Ra_{bl} \approx 50$ was found for the quasi-steady run-down of the two-dimensional simulation of Carpenter *et al.* (2012), showing reasonable agreement with the three-dimensional results found here.

7. Summary and conclusions

A series of DNS have been performed to study the diffusive interface within the range of conditions found in geophysical observations, notably the thermohaline staircase of Lake Kivu. The boundary conditions correspond to previous laboratory

studies, which are carried out in a container insulated against the flux of T and S. The DNS therefore exhibit a time-dependent 'run-down' of the T and S differences across the interface.

The simulations provide the most detailed observations of the diffusive interface to date, and have revealed a number of important features. The *TS*-interfaces are found to evolve naturally to a double-boundary-layer structure where the T-interface is thicker than the S-interface, i.e. $r \equiv h_T/h_S > 1$. Therefore, two gravitationally unstable boundary layers are supported on each side of the stably stratified central core of the interface. These unstable boundary layers were found to lead to the formation of plumes that feed large-scale convection cells within the mixed layers. This circulation creates a shear across the boundary layers with a reduced shear inside the interface core. By accounting for the shear across the boundary layers, various scaling laws can be obtained to predict the interface thickness ratio r based on the diffusivity ratio τ. Using the observed shear profiles in the boundary layer we find that $r \sim \tau^{-1/5}$ best describes the simulations, and is consistent with our observed scaling.

The turbulence of the mixed layers was not found to penetrate the stable stratification of the core, and the *TS*-fluxes were reduced to molecular levels inside the interface. Once a quasi-steady run-down state was achieved, the evolution of the interface thicknesses, and therefore also the fluxes, were found to be well-predicted by the model of Newell (1984), which assumes that the S-interface thickness is governed by pure molecular diffusion of the interface in time. This model is also consistent with the more general formulation of Worster (2004). The flux ratio $R_F \equiv F_S/F_T$ was predicted well by the ratio of T and S molecular fluxes $R_F = r\tau R_\rho$, where the density ratio R_ρ is determined by the run-down of the mixed layers, and $r \sim \tau^{-1/5}$ was found to be approximately constant in time for each simulation.

Finally, we considered the stability of the boundary layers as a function of the boundary layer Rayleigh number Ra_{bl}. We found that an order-of-magnitude estimate of $Ra_{bl} = O(10^2)$ can be used to describe the simulations. However, we remark that the boundary layer stability may be inherently time-dependent and may exhibit a dependence on the circulations that develop. In this case, a critical boundary layer Rayleigh number would not apply to all diffusive interfaces (see Carpenter *et al.* 2012, for further discussion).

Future work could extend the present DNS in several ways. For example, the run-down behaviour of the interface could possibly be removed by including periodic conditions at the top and bottom boundaries, also bringing the simulations closer to conditions found in natural staircases, and this work is currently underway. Also, more simulations could be performed to test the scaling relationship between r and τ. A future study should also investigate the low-R_ρ regime in which mixed-layer turbulence is expected to penetrate the interface and alter the coupled transports of T and S. Finally, a more accurate description of the stability properties of the diffusive interface might be possible by explicitly including the time-dependent interface growth.

Acknowledgements

We would like to thank M. Schmid, M.-L. Timmermans, and M. Toffolon for helpful discussions, and B. Smyth and K. Winters for providing the DNS code for the simulations. The manuscript has greatly benefitted from the comments of the anonymous referees. This project has been supported by the Swiss National Science Foundation grant 200021-122183 (Lake Kivu – turbulence and double diffusion in permanent stratification). The Swiss National Science Foundation is also acknowledged

for partly financing the IPAZIA computational cluster (project 206021-128754). Part of the salary of the first author was made possible by the EU project grant 263287 (FreshMon – High Resolution Freshwater Monitoring: FreshMon GMES Downstream Services).

REFERENCES

BAINES, P. G. & GILL, A. 1969 On thermohaline convection with linear gradients. *J. Fluid Mech.* **34**, 289–306.

BATCHELOR, G. K. 1959 Small-scale variation of convected quantities like temperature in turbulent fluid. *J. Fluid Mech.* **5**, 113–133.

CARO, G. P. 2009 Direct numerical simulations of diffusive staircases in the Arctic. Master's thesis, Naval Postgraduate School.

CARPENTER, J. R., SOMMER, T. & WÜEST, A. 2012 Stability of a double-diffusive interface in the diffusive convection regime. *J. Phys. Oceanogr.* **42**, 840–854.

CRAPPER, P. F. 1975 Measurements across a diffusive interface. *Deep-Sea Res.* **22**, 537–545.

FERNANDO, H. J. S. 1989 Buoyancy transfer across a diffusive interface. *J. Fluid Mech.* **209**, 1–34.

GROSSMAN, S. & LOHSE, D. 2000 Scaling in thermal convection: a unifying theory. *J. Fluid Mech.* **407**, 27–56.

HOARE, R. A. 1966 Problems of heat transfer in Lake Vanda, a density stratified Antarctic Lake. *Nature* **210**, 787–789.

HOWARD, L. N. 1964 Convection at high Rayleigh number. In *Proc. 11th Intl Cong. Appl. Mech*. Springer, pp. 1109–1115.

HUPPERT, H. E. & SPARKS, R. S. J. 1984 Double-diffusive convection due to crystallization in magmas. *Annu. Rev. Earth Planet. Sci.* **12**, 11–37.

KELLEY, D. E. 1990 Fluxes through diffusive staircases: a new formulation. *J. Geophys. Res.* **95**, 3365–3371.

KELLEY, D. E., FERNANDO, H. J. S., GARGETT, A. E., TANNY, J. & ÖZSOY, E. 2003 The diffusive regime of double-diffusive convection. *Prog. Oceanogr.* **56**, 461–481.

KIMURA, T. & SMYTH, W. D. 2007 Direct numerical simulation of salt sheets and turbulence in a double-diffusive shear layer. *Geophys. Res. Lett.* **34**, L21610.

LINDEN, P. F. 2000 Convection in the environment. In *Perspectives in Fluid Dynamics* (ed. G. K. Batchelor, H. K. Moffatt & M. G. Worster), pp. 289–345. Cambridge University Press.

LINDEN, P. F. & SHIRTCLIFFE, T. G. L. 1978 The diffusive interface in double-diffusive convection. *J. Fluid Mech.* **87**, 417–432.

MARMORINO, G. O. & CALDWELL, D. R. 1976 Heat and salt transport through a diffusive thermohaline interface. *Deep-Sea Res.* **23**, 59–67.

MOIN, P. & MAHESH, K. 1998 Direct numerical simulation: a tool in turbulence research. *Annu. Rev. Fluid Mech.* **30**, 539–578.

MOLEMAKER, M. J. & DIJKSTRA, H. A. 1997 The formation and evolution of a diffusive interface. *J. Fluid Mech.* **331**, 199–229.

NEAL, V. T., NESHYBA, S. & DENNER, W. 1969 Thermal stratification in the Arctic Ocean. *Science* **166**, 373–374.

NEWELL, T. A. 1984 Characteristics of a double-diffusive interface at high density stability ratios. *J. Fluid Mech.* **149**, 385–401.

NOGUCHI, T. & NIINO, H. 2010*a* Multi-layered diffusive convection. Part 1. Spontaneous layer formation. *J. Fluid Mech.* **651**, 443–464.

NOGUCHI, T. & NIINO, H. 2010*b* Multi-layered diffusive convection. Part 2. Dynamics of layer evolution. *J. Fluid Mech.* **651**, 465–481.

PADMAN, L. & DILLON, T. M. 1987 Vertical heat fluxes through the Beaufort Sea thermohaline staircase. *J. Geophys. Res.* **92**, 10,799–10,806.

PADMAN, L. & DILLON, T. M. 1989 Thermal microstructure and internal waves in the Canada Basin diffusive staircase. *Deep-Sea Res.* **36**, 531–542.

SANCHEZ, X. & ROGET, E. 2007 Microstructure measurements and heat flux calculations of a triple-diffusive process in a lake within the diffusive layer convection regime. *J. Geophys. Res.* **112**, C02012.

SCHMID, M., BUSBRIDGE, M. & WÜEST, A. 2010 Double-diffusive convection in Lake Kivu. *Limnol. Oceanogr.* **55** (1), 225–238.

SCHMID, M., LORKE, A., DINKEL, C., TANYILEKE, G. & WÜEST, A. 2004 Double-diffusive convection in Lake Nyos, Cameroon. *Deep-Sea Res.* **51**, 1097–1111.

SHIRTCLIFFE, T. G. L. 1973 Transport and profile measurements of the diffusive interface in double diffusive convection with similar diffusivities. *J. Fluid Mech.* **57**, 27–43.

SMYTH, W. D. & MOUM, J. N. 2000 Length scales of turbulence in stably stratified mixing layers. *Phys. Fluids* **12** (6), 1327–1342.

SMYTH, W. D., MOUM, J. N. & CALDWELL, D. R. 2001 The efficiency of mixing in turbulent patches: Inferences from direct simulations and microstructure observations. *J. Phys. Oceanogr.* **31**, 1969–1992.

SMYTH, W. D., NASH, J. D. & MOUM, J. N. 2005 Differential diffusion in breaking Kelvin–Helmholtz billows. *J. Phys. Oceanogr.* **35**, 1004–1022.

SOMMER, T., CARPENTER, J. R., SCHMID, M., LUECK, R. & WÜEST, A. 2013 Revisiting microstructure sensor responses with implications for double-diffusive fluxes. *J. Atmos. Ocean. Technol.* (submitted).

STAMP, A. P., HUGHES, G. O., NOKES, R. I. & GRIFFITHS, R. W. 1998 The coupling of waves and convection. *J. Fluid Mech.* **372**, 231–271.

STERN, M. E. 1960 The salt-fountain and thermohaline convection. *Tellus* **2**, 172–175.

TAKAO, S. & NARUSAWA, U. 1980 An experimental study of heat and mass transfer across a diffusive interface. *Intl J. Heat Mass Transfer* **23**, 1283–1285.

TIMMERMANS, M.-L., TOOLE, J., KRISHFIELD, R. & WINSOR, P. 2008 Ice-tethered profiler observations of the double-diffusive staircase in the Canada Basin thermocline. *J. Geophys. Res.* **113**, C00A02.

TURNER, J. S. 1965 The coupled turbulent transports of salt and heat across a sharp density interface. *Intl J. Heat Mass Transfer* **8**, 759–767.

TURNER, J. S. 1973 *Buoyancy Effects in Fluids*. Cambridge University Press.

TURNER, J. S., SHIRTCLIFFE, T. G. L. & BREWER, P. G. 1970 Elemental variations of transport coefficients across density interfaces in multiple-diffusive systems. *Nature* **228**, 1083–1084.

VERONIS, G. 1965 On finite amplitude instability in thermohaline convection. *J. Mar. Res.* **23**, 1–17.

WINTERS, K. B. & D'ASARO, E. A. 1996 Diascalar flux and the rate of fluid mixing. *J. Fluid Mech.* **317**, 179–193.

WINTERS, K. B., LOMBARD, P. N., RILEY, J. J. & D'ASARO, E. A. 1995 Available potential energy and mixing in density-stratified fluids. *J. Fluid Mech.* **289**, 115–128.

WINTERS, K. B., MACKINNON, J. A. & MILLS, B. 2004 A spectral model for process studies of rotating, density-stratified flows. *J. Atmos. Ocean. Technol.* **21**, 69–94.

WORSTER, M. G. 2004 Time-dependent fluxes across double-diffusive interfaces. *J. Fluid Mech.* **505**, 287–307.